
This article has been peer-reviewed and is now freely available (open access) at *Tectonophysics*: <https://doi.org/10.1016/j.tecto.2026.231100>. This version submitted to EarthArXiv reflects the final revised version submitted to the journal.

Please cite as:

Haag, M.B., Jess, S., Schoenbohm, L.M., Enkelmann, E., Pinto, T.F., 2026. Long-lived topography along rifted margins: Insights from Aparados da Serra escarpment, Southeast Brazil. *Tectonophysics* 925, 231100. <https://doi.org/10.1016/j.tecto.2026.231100>

Please forward questions and feedback to mbhaag@mit.edu

LONG-LIVED TOPOGRAPHY ALONG RIFTED MARGINS: INSIGHTS FROM APARADOS DA SERRA ESCARPMENT, SOUTHEAST BRAZIL

Mauricio B. Haag^{1,2*}, Scott Jess^{2,3}, Lindsay M. Schoenbohm^{1,2}, Eva Enkelmann⁴, Taís F. Pinto⁴

¹ Department of Earth Sciences, University of Toronto, Toronto, ON, Canada

² Department of Chemical and Physical Sciences, University of Toronto Mississauga, Mississauga, ON, Canada

³ School of the Environment, Washington State University, Pullman, WA, USA

⁴ University of Calgary, Department of Earth, Energy, and Environment, Calgary, AB, Canada

Mauricio B. Haag (<https://orcid.org/0000-0001-5038-4418>)

Lindsay M. Schoenbohm (<https://orcid.org/0000-0001-7898-356X>)

Scott Jess (<https://orcid.org/0000-0003-1960-2901>)

Eva Enkelmann (<https://orcid.org/0000-0002-1988-0760>)

Taís F. Pinto (<https://orcid.org/0009-0003-4762-9156>)

ABSTRACT

The Brazilian margin is one of the longest elevated passive margins (EPMs) in the world. However, both the timing of uplift and the long-term evolution of this EPM remain highly debated. In this study, we present a new suite of apatite (U-Th-Sm)/He (AHe) and fission track (AFT) ages for the southern end of the Brazilian EPM, in the Aparados da Serra plateau. Combined with literature data, our results reveal that mean AHe ages range from 43 – 112 Ma, while AFT ages range from 46 – 222 Ma. Thermal history models suggest monotonic exhumation rates in the Aparados da Serra, with post-rifting rates $< 50 \text{ m Myr}^{-1}$ in the coastal plain and $< 25 \text{ m Myr}^{-1}$ in the volcanic plateau. Collectively, our results imply a total erosion of 2 – 4 km of material from the coast and $< 2 \text{ km}$ from the plateau since rifting ca. 120 – 100 Ma. AHe and AFT data indicate no detectable accelerated phase of exhumation during the Cenozoic, implying that recent uplift along the margin was either absent or minimal, and that

the relief observed in the Aparados da Serra is likely a consequence of sustained rift topography. Based on the absence of major recent tectonic events, we argue that Cenozoic exhumation patterns in the Aparados da Serra were largely controlled by geomorphologic processes (e.g., differential erosion). Lastly, the equivalence between long (AFT and AHe) and short-term (catchment-averaged) erosion rates argues for sustained stability of the margin over geological timescales.

1 INTRODUCTION

Elevated passive margins (EPMs) represent the most dynamic regions within passive tectonic settings, featuring maximum erosion rates that are comparable to those in tectonically active regions (Wang et al., 2021). Despite significant research into the role of post-break-up deformation, uplift, and erosion along EPMs (e.g., Gallagher et al., 1994; van der Beek et al., 2002; Japsen et al., 2012; Braun, 2018; Hueck et al., 2019), fundamental questions about the timing of uplift and long-term geomorphic evolution of these settings remain controversial (Braun, 2018; Fonte-Boa et al., 2022; Danišík & Kirkland, 2023). One central debate concerns whether present-day EPM topography largely reflects preserved rift relief maintained by lithospheric flexure and isostatic support (e.g., Nielsen et al., 2009; Jess et al., 2019, 2020; Sacek et al., 2019; Silva and Sacek, 2019), or whether it results from episodic post-rift uplift, erosion, and peneplanation cycles (e.g., Japsen et al., 2012; Green et al., 2022). In addition to these geodynamic processes, the dominant geomorphic processes responsible for EPM degradation remain debated, particularly whether erosion occurs mainly through progressive plateau degradation or through headward escarpment retreat (van der Beek et al., 2002; Braun & van der Beek, 2004; Braun, 2018).

The southeast Brazilian continental margin comprises one of the longest EPMs on Earth (Fonte-Boa et al., 2022). This margin features a series of 1 – 3 km asl escarpment systems stretching for nearly 2,000 km along the South Atlantic coast (Fig. 1A), with striking structural and lithologic diversity (Fonte-Boa et al., 2022). The southern end of this system (south of lat. 28°S), hereafter named Aparados da Serra, is distinct from other segments of the EPM due to its extremely low-relief plateau (Fig. 1B-C), elevated topography (~ 1 km asl), and absence of post-break-up volcanism or reactivation, which are common features along other parts of the Brazilian EPM (Riccomini et al., 1989; Cogné et al., 2012; Sacek et al., 2012; Fonte-Boa et al., 2022; Fonseca et al., 2023). Despite these distinctive characteristics, the exhumation history of the Aparados da Serra remains poorly constrained, as thermochronological studies have predominantly focused on the northern segment of the Brazilian EPM (Fig. 1D-E).

In this study, we present a suite of apatite (U-Th-Sm)/He (AHe) and fission track (AFT) dates for the Aparados da Serra (Fig. 1E). Combined with geological observations, inverse thermal history models are compatible with a protracted exhumation histories since rifting at ca. 120 - 100 Ma. These results indicate that the present-day elevated topography of the Aparados da Serra does not require significant Cenozoic uplift and can instead be explained by long-term denudation following Cretaceous rifting. Lastly, the spatial distribution and range of AHe ages show some correspondence with an escarpment-retreat hypothesis; however, the limited number of samples and the absence of a clearly resolved cooling wave prevent a definitive assessment of denudation style. Collectively, these results provide new constraints on the long-term evolution of southern Brazilian elevated passive margins.

2 GEOLOGICAL BACKGROUND

Located at the southern limit of the Brazilian EPM, the Aparados da Serra consists of a volcanic plateau (1.0 – 1.6 km asl) bounded to the east by a 200-km long NNE-SSW-trending escarpment (Fig. 2). From north to south, the escarpment morphology transitions from a simple, “divide-type escarpment” in which the divide and scarp edge are coincident and sub-linear to a more complex and sinuous “gorge-head type” escarpment, marked by a series of embayments and deeply incised fluvial valleys (Fig. 2) (Haag et al. 2025b). This trend is accompanied by a decrease in the distance between the escarpment and the coast, which gradually declines from ~ 90 km in the north to 15 km in the south (Fig. 2).

Geological units are divided into three major groups along the Aparados da Serra, from older to recent: (i) underlying basement units include plutonic and metamorphic rocks (Ediacaran) of the Dom Feliciano Belt (Brasiliano Orogeny); (ii) overlying clastic (marine – fluvial) sedimentary rocks of the Paraná Basin (Lower Permian - Cretaceous); and (iii) capping effusive volcanics of the Paraná-Etendeka LIP (lower Cretaceous), locally grouped in the Serra Geral Group (Milani et al., 2007; Canile et al., 2016; Rossetti et al., 2018; Gomes & Vasconcelos, 2021; Salazar-Mora and Sacek, 2023; Scherer et al., 2023). In the study area, the escarpment is mainly composed of volcanic and sedimentary rocks, while basement units are restricted to the lower coastal domains. No younger lithological units have been identified overlying the plateau or along the escarpment face (Wildner 2008, 2014). This absence may reflect either non-deposition of post-rift sedimentary units or their complete removal by erosion since rifting.

Tectonically, the study area evolved from an orogenic collisional setting (Pan-African/Brasiliano, Neoproterozoic) to a large intra-cratonic basin (Ordovician–Cretaceous), characterized by the deposition of thick sedimentary units of the Paraná Basin (Milani et al., 2007; Scherer et al., 2023). The geological record of the Paraná Basin is characterized by extensive periods of exhumation (e.g., Lower Triassic–Upper Jurassic), as indicated by several unconformities within the basin (Milani et al., 2007; Canile et al., 2016; Scherer et al., 2023). Relevant to this study, the late tectonic history (Cretaceous–Present) includes the emplacement of the Paraná-Etendeka LIP, resulting in the deposition of > 2 km of lavas (Milani et al., 2007; Rossetti et al., 2018; Gomes & Vasconcelos, 2021; Krob et al., 2019). The emplacement of the Paraná -Etendeka LIP was followed shortly by the opening of the South Atlantic through rifting, establishing a passive margin in the region at ~ 120–100 Ma (Contreras et al., 2010; Stica et al., 2014).

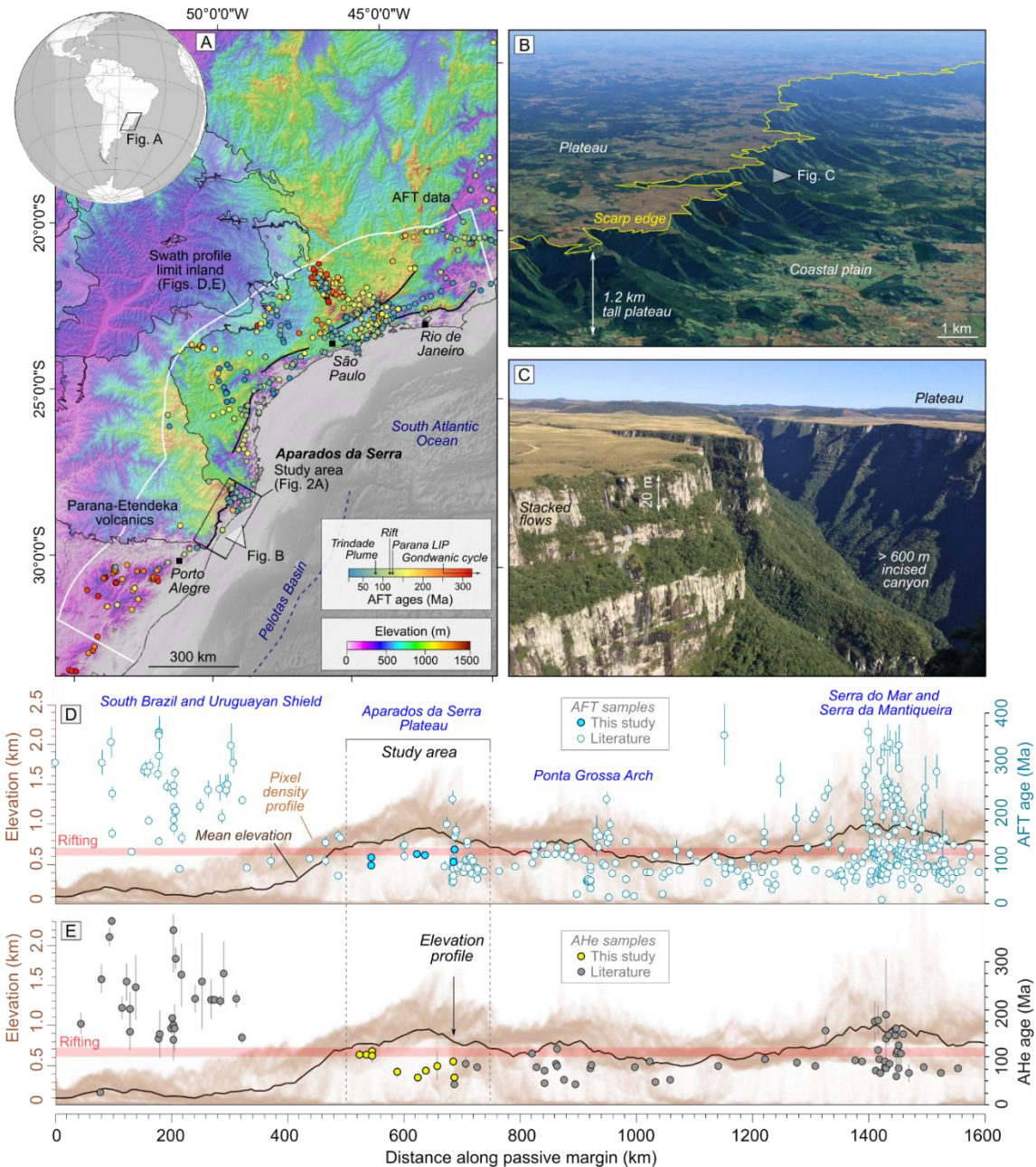


Figure 1 – A) Topographic setting of the southeast Brazilian passive margin and the available AFT cooling ages; B) GoogleEarth view of the central segment of Aparados da Serra; C) Field photo of deeply incised canyons along the south limit of the study area; D-E) 300-km wide elevation swath profile (left axis) along the passive margin, from the Uruguayan Shield to the Serra do Mar and Serra da Mantiqueira ridges, along with the available (D) AFT cooling ages (right axis) and (E) AHe cooling ages (right axis). The AFT panel includes data compiled from [Krob et al. \(2020\)](#), while AHe includes data from [Karl et al. \(2013\)](#), [Krob et al. \(2019\)](#), [Cogné et al., \(2011, 2012\)](#), [Hueck et](#)

al. (2019), Machado et al. (2019, 2020), and Gezatt et al. (2021). In D and E, pixel density represents terrain elevation. The timing of rifting is indicated with a horizontal red line at an age of 100 - 120 Ma.

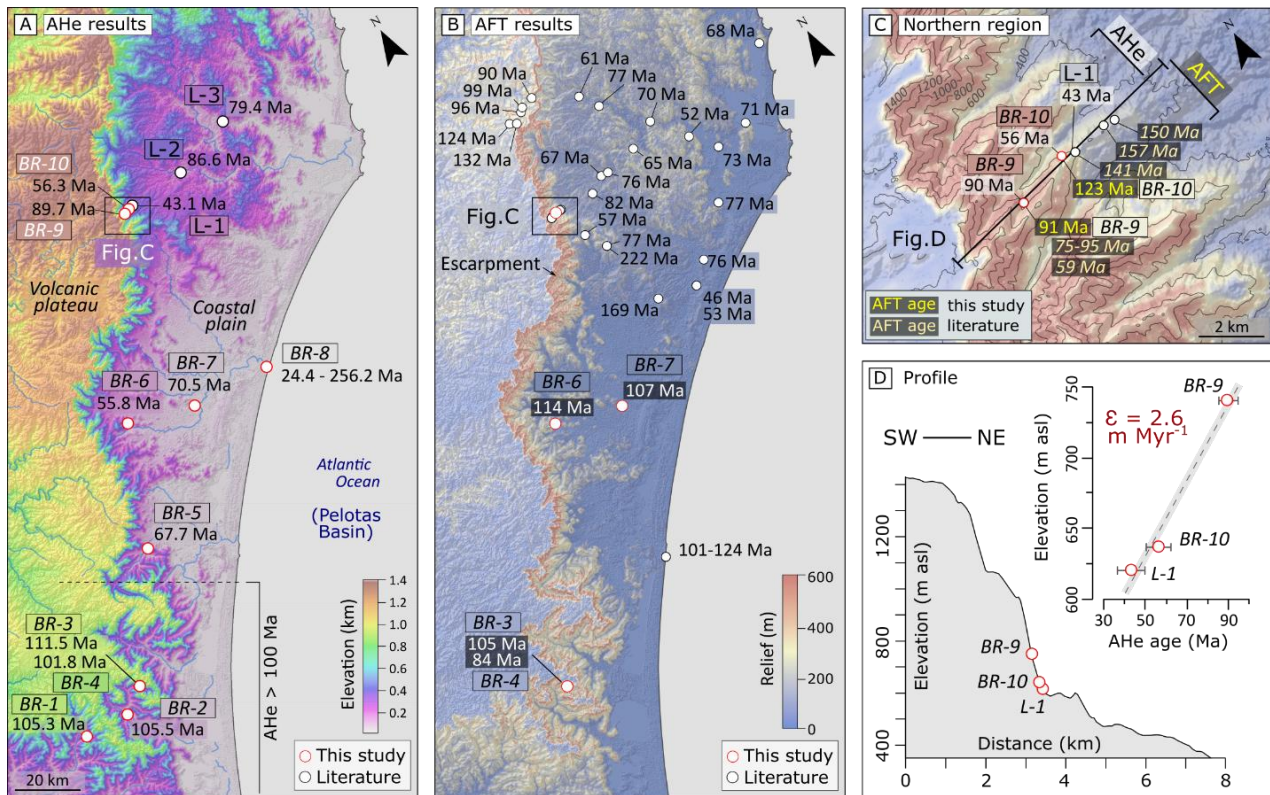


Figure 2 – A) Topography of the study area with the respective AHe cooling ages. B) Relief of the study area with respective available AFT central ages. C) Inset of the northern section of the study area (Rio do Rastro Profile) highlighting AHe and AFT ages; D) Cross section on escarpment edge with respective AHe sample locations. Samples from the literature include data from Gallagher et al. (1994), Karl et al. (2013), Krob et al. (2019) and Bicca et al. (2020). A geological map is provided in SI1.

3 METHODS

To resolve the exhumation history of the study area we combine apatite low-temperature thermochronology techniques, apatite (U–Th)/He (AHe) and apatite fission-track (AFT), with thermal history modeling. All analytical procedures were performed at the Calgary Geo- and

Thermochronology Laboratory of the University of Calgary and follow the methods summarized by [McKay et al. \(2021\)](#) for AHe analysis and [Fraser et al. \(2021\)](#) for AFT analysis.

3.1 Sampling strategy

Sampling focused on transects perpendicular to the escarpment face, along one elevation profile, and at several control points along the escarpment face and coastal plain ([Fig. 2A](#)). In this contribution, all samples are collected from sedimentary units of the Paraná Basin, including: Botucatu Fm. (Early Cretaceous; medium to fine eolian sandstone; [Scherer, 2000](#)), with a depositional age of 134 – 145 Ma ([Bertolini et al., 2020](#)) and U-Pb peak in zircon provenance ages of Ediacaran age ([Canile et al., 2016](#); [Bertolini et al., 2021](#)); and Rio do Rastro Fm. (Permian–Triassic; fine sandstones interbedded with siltstone and mudstones; [Canile et al., 2016](#)), with a depositional age of 250 – 280 Ma ([Milani et al., 2007](#); [Canile et al., 2016](#)) and U-Pb zircon provenance of Ediacaran age ([Canile et al., 2016](#)). For details on sampling sites, please check SI1. For each sample, we collected 2 – 5 kg of material for mineral processing, which was performed at the University of Toronto Mississauga, following the approach of [Donelick \(2005\)](#). Please refer to SI2 for details on mineral separation.

In addition to our own AHe and AFT data, we also include three AHe samples from [Karl et al. \(2013\)](#) and forty AFT samples from [Gallagher et al. \(1994\)](#), [Karl et al. \(2013\)](#), [Krob et al. \(2019\)](#), and [Bicca et al. \(2020\)](#) in our data analysis ([Fig. 2](#)). These studies include sedimentary samples from the Rio Bonito Fm. (Carboniferous–Permian; fine sandstones interbedded with siltstone and mudstones; [Canile et al., 2016](#)), volcanics from the Serra Geral Gr., as well as granitoid samples from basement rocks (Ediacaran).

3.2 Apatite (U-Th-Sm)/He

We focus on AHe analysis due to its low-temperature sensitivity with the partial retention zone for helium (HePRZ) ranging from 40 – 70°C (e.g., [Flowers et al., 2009](#)), suitable for analyzing near-surface (1 – 2 km) processes (e.g., [van der Beek et al., 2002](#); [Braun & van der Beek, 2004](#)). In this contribution, we present AHe ages for a total of ten samples ([Table 2](#)). For each sample, whenever possible, we select well-formed, unbroken, inclusion-free crystals using a Stereo Microscope model ZEISS SteREO Discovery.V12 (SI3). We then picked five to seven crystals from this pool, recording each crystal's length, long width, short width, number of terminations, and surface aspects. Lastly, we packed individual grains in Nb tubes and performed the He extraction using an Applied Spectra Alphachron helium line, while parent isotopes (^{235}U , ^{238}U , ^{232}Th , and ^{147}Sm) were determined via isotope dilution ([Evans et al., 2005](#)). We calculated ages using the Taylor expansion method and corrected for alpha ejection using the approach of [Ketcham et al. \(2011\)](#). Analytical results are reported in the SI3.

3.3 Apatite Fission Track

We selected six samples for AFT dating using laser ablation fission track analysis (LA-AFT) ([Hasebe et al., 2004](#)). AFT dating is sensitive to slightly higher temperatures when compared to AHe, with the fission track partial annealing zone (PAZ) ranging 60–120°C (e.g., [Gallagher et al., 1998](#)). We mounted and polished the selected samples, followed by standard etching protocol of 5.5M HNO_3 at 21°C for 20 seconds ([Donelick, 2005](#)). A detailed description of sample preparation is provided by [Fraser et al. \(2021\)](#). We aimed to date 30 grains per sample and measured the diameter of the track opening parallel to the c-axis (D_{par}) to gain

information on apatite kinetic parameters (Ketcham et al., 2007). The grains chosen for dating had homogeneous track distribution, no fractures and no inclusions. Spontaneous track counting was performed in a Zeiss Axiomager.M2m optical microscope equipped with an Autoscan System Pty. Ltd. Stage. Similarly, confined track lengths measurements were conducted and are reported in SI4. U concentration measurement was performed using an Applied Spectra Resolution LR Laser Ablation System coupled to an Agilent 7700x Quadrupole ICP-MS. Ablation spots were 33 μ m in diameter and placed in the center of the area where spontaneous tracks were counted. The fission track ages were calculated and zeta calibrated using the equations outlined by Hasebe et al. (2004, 2013). Durango apatite standards were frequently analyzed throughout the laser ablation session to ensure proper zeta calculation. Additionally, NIST610 was analyzed for calculation of uranium concentrations. Complete AFT data analysis results (analytical results, radial plots, length measurements and Dpar) are reported in SI4.

3.4 Thermal history modelling

We combined AHe and AFT cooling ages, track length, compositional data, and independent geological constraints to perform inverse thermal history modeling using *QTQt* 5.8.6 (Gallagher, 2012), thereby testing the consistency of the known geological evolution against the thermochronological dataset. *QTQt* uses a Markov Chain Monte Carlo (MCMC) approach to obtain a set of “acceptable” thermal histories. For each model, we secure algorithm stability by performing runs with at least 1 million iterations, ensuring a steady likelihood chain (Gallagher, 2012). Additionally, samples located within the same region and without evidence of tectonic displacement (e.g., BR-9, 10 and L-1; Fig. 2) are modelled as a

group. Thermal histories modelling was only completed on samples with both AFT and AHe data (BR-3, 4, 6, 7, 9, and 10), or on those AHe samples that could be included in a joint inversion with other samples (e.g., BR-1, 2, and L-1). Initial modeling attempts using exclusively AHe data (BR-5 and 8) revealed data dispersion that was too high to yield meaningful results. In the inverse modelling, we exclude three grains (BR-4d, BR-7c, and BR-8e) due to anomalously high Th and Sm contents and because they fall outside expected parent–daughter trends (SI3; Fig. S3.5) (Härtel et al., 2022).

Table 1 – Inputs for the thermal model. H_p indicates the plateau elevation, while H_s the sample elevation, in km.

* The timing at which the Rio do Rastro Formation first approached near-surface conditions remains poorly constrained and may have occurred as early as ~200 Ma. However, prescribing a near-surface timing of 140 Ma does not affect the model results, because the model has sufficient freedom to evolve toward shallow crustal temperatures regardless of the exact timing.

Timing	Event Class	Affected units	Temperature	References
0 Ma	Present day temperature	All units	$20 \pm 10 \text{ }^\circ\text{C}$	Wygrala (1989)
$133 \pm 1 \text{ Ma}$	Depositional	Serra Geral Gr. (Paraná-Etendeka LIP)	$T_{\text{MIN}} = (H_p - H_s) \times 30^\circ\text{C}$ $T_{\text{MAX}} = \text{Unconstrained}$	Gomes & Vasconcelos (2021)
$140 \pm 6 \text{ Ma}$	Depositional	Botucatu Fm.	$20 \pm 10 \text{ }^\circ\text{C}$	Milani et al. (2007) ; Canile et al. (2016) ; Bertolini et al. (2020) .
	Exhumation*	Rio do Rastro Fm.		
$265 \pm 15 \text{ Ma}$	Depositional	Rio do Rastro Fm.	$20 \pm 10 \text{ }^\circ\text{C}$	
$580 \pm 80 \text{ Ma}$	Provenance	All sedimentary units	$800 \pm 200 \text{ }^\circ\text{C}$	

We performed joint inversion of AFT and AHe data using the fission-track annealing model of [Ketcham et al. \(2007\)](#) and the diffusion model of [Gautheron et al. \(2009\)](#). Single-grain

AHe age dispersion is expected in detrital samples that may have experienced prolonged residence in the HePRZ (e.g., [Jess et al., 2019](#)). Considering that all samples in our dataset are detrital and likely resided for extended periods within the HePRZ ([Gallagher et al., 1994](#); [Karl et al., 2013](#); [Krob et al., 2019](#); [Bicca et al., 2020](#)), we implemented additional steps to better account for kinetic variability in thermal modeling: (i) we applied the radiation damage model ([Gautheron et al., 2009](#); [Recanati et al., 2017](#)) to account for changes in helium diffusivity, and (ii) we resampled the additional activation energy (ΔE_b) required for diffusion of helium trapped in damage vacancies ([Gautheron et al., 2009, 2012](#); [Gerin et al., 2017](#)). Accordingly, while the radiation damage model seeks to compensate for changes in diffusion kinetics, resampling ΔE_b between 20 – 50 kJ mol⁻¹ seeks to improve model predictions by accounting for different apatite composition and damage ([Gerin et al., 2017](#)). See SI6 for further details in inverse thermal history modelling.

The Paraná Basin has been extensively studied due to the presence of mineral resources including coal and gas (e.g., [Milani et al., 2007](#); [Bicca et al., 2020](#)). This detailed tectonic and stratigraphic framework allows us to independently constrain thermal events, including depositional and exhumation periods outlined in [Table 1](#). The present-day geothermal gradient in the study area ranges from 30 – 35°C km⁻¹ ([Vieira & Hamza, 2019](#)) but was likely higher during the emplacement of the Paraná-Etendeka LIP and subsequent rifting. Accordingly, total overburden and erosion rates are estimated from cooling rates using geothermal gradient from 30 – 40°C km⁻¹.

4 RESULTS

We report a total of 51 new AHe dates from ten samples and AFT dates from six samples ([Table 2](#)). In our samples, single-grain AHe data range from 18 – 254 Ma, while mean AHe sample ages range 56 – 111 Ma. AFT central ages range from 84 – 123 Ma, with MTL of 13.31 – 14.38 μm and Dpar of 1.93 – 2.66 μm ([Table 2](#)). All AFT samples show high dispersion with P (χ^2) < 0.05.

4.1 Apatite low-temperature thermochronology

Including data from [Karl et al. \(2013\)](#), the mean AHe sample ages range from 43 – 112 Ma ([Fig. 3B](#), S17) in the study area. We group AHe data based on their sampling location ([Fig. 3A](#)):

- (i) **Deep-incised valleys** (four samples, BR-1 to 4): samples located at low elevations landward of the escarpment crest, at the bottom of narrow and deep fluvial valleys cut into the plateau and located in the southern part of the study area ([Fig. 2A, 3A](#)). These samples are typically older (\sim rift age), with mean AHe ages ranging 102 – 111 Ma ([Fig. 3B](#)).
- (ii) **Escarpment face** (three samples, BR-9, 10 and L-1): collected on the escarpment face ([Fig. 2A, 3A](#)), these samples display a wide range of mean AHe ages from 43 – 90 Ma ([Karl et al., 2013](#)) and are younger than rifting (< rift age) ([Fig. 3B](#)). These samples show a positive correlation between sample elevation and AHe age ([Fig. 2D](#)).
- (iii) **Coastal plain** (six samples, BR-5 to 8, L2 and L3): collected between the coastline and the escarpment foot ([Fig. 2A, 3A](#)), these samples also feature variable ages

and are relatively young (< rift age), with mean AHe ages from 56 – 87 Ma (Karl et al., 2013) (Fig. 3B). Spatially, AHe ages are marked by a younging trend from the coast toward the escarpment, although significant variability is present (Fig. 3B).

Combined with samples from the literature (Gallagher et al. 1994; Karl et al. 2013; Krob et al. 2019; Bicca et al. 2020; SI7), AFT central ages range from 46 – 222 Ma, without a distinct spatial distribution (Fig. 3C, 4B). MTLs range from 10.3 to 15.1 μm (Fig. 4C); overall, volcanic samples from higher elevations, reported by Gallagher et al. (1994) feature longer length measurements (MTL > 14.1 μm), while sedimentary and basement samples show a spread of MTL values from 12.3 – 14.4 μm (Fig. 4C, SI7).

1 **Table 2** – Thermochronology results. Sample elevation, stratigraphic age, and the distance to the coastline. For AHe and AFT results, N represents
 2 the number of grains analyzed; For track length results, N represents the number of measured tracks. MTL results are reported as corrected for c-axis. For
 3 AHe data, a complete table with analytical results, grain measurements, uncorrected ages and Ft correction is reported in SI3. For AFT data, complete
 4 information regarding analytical results, radial plots, MTL and Dpar measurements are reported in SI4.

Sample information				AHe results (corrected)			AFT results			Track length results		
Lithologic unit	Sample ID	Z (m asl)	Distance to coast (km)	N	Min – Max (Ma)	Mean age ± σ_1 (Ma)	N	Central age ± σ_1 error (Ma)	Dispersion	N	Projected MTL ± σ_1 (μm)	Dpar ± σ_1 (μm)
Botucatu Fm. Early Cretaceous	BR-1	145	40	5	74 – 131	105.3 ± 10.8	-	-	-	-	-	-
	BR-2	71	29	5	82 – 130	105.5 ± 8.2	-	-	-	-	-	-
	BR-3*	261	27	5	75 – 154	111.5 ± 13.2	28	105 ± 12	23%	32	13.31 ± 0.25	2.14 ± 0.29
	BR-4	260	27	4	18 – 122	101.7 ± 14.1	30	84 ± 14	40%	12	14.15 ± 0.23	1.93 ± 0.15
	BR-5	127	30	4	45 – 197	67.7 ± 10.0	-	-	-	-	-	-
	BR-9*	740	50	5	78 – 106	89.7 ± 4.6	29	91 ± 11	28%	46	14.16 ± 0.13	2.21 ± 0.18
Rio do Rastro Fm. Upper Permian	BR-6	131	41	4	44 – 161	55.7 ± 8.0	26	114 ± 18	33%	95	14.27 ± 0.11	2.33 ± 0.44
	BR-7	12	21	3	32 – 75	70.5 ± 2.7	32	107 ± 17	39%	54	14.38 ± 0.14	2.66 ± 0.43
	BR-8	30	1	7	24 – 254	-	-	-	-	-	-	-
	BR-10	637	49	5	43 – 76	53.6 ± 6.0	17	123 ± 12	30%	70	13.72 ± 0.16	2.35 ± 0.32

5 * Samples collected within 1 m of the lava-sandstone contact.

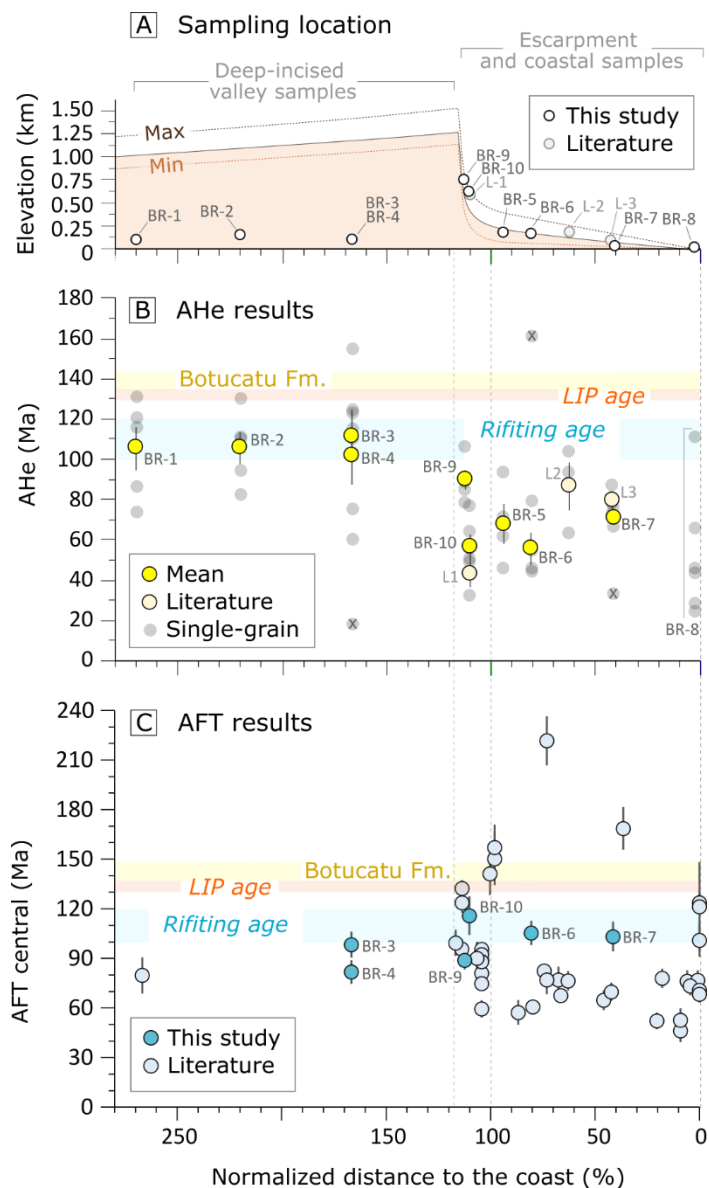


Figure 3 – Geographic distribution of AHe and AFT ages. The x-axis shows the normalized distance between the coastline and the escarpment top, where 0% corresponds to samples collected at the coast, 50% to the midpoint, 100% to the escarpment bottom (relief < 200m/km), and values >100% indicate locations landward of the escarpment. A) Generalized, present-day escarpment morphology with sample location and altitude. B) Mean AHe cooling ages. C) AFT central ages. The main tectonic and depositional events are represented in B-C by horizontal bars and include the deposition of Botucatu Formation ca. 140 Ma (Bertolini et al., 2020), the Paraná-Etendeka LIP lavas ca. 133 Ma (Gomes and Vasconcelos, 2021), the opening of the South Atlantic

Ocean ca. 120 – 100 Ma (Stica et al., 2014). The samples from the literature include data from Gallagher et al. (1994), Karl et al. (2013), Krob et al. (2019), and Bicca et al. (2020).

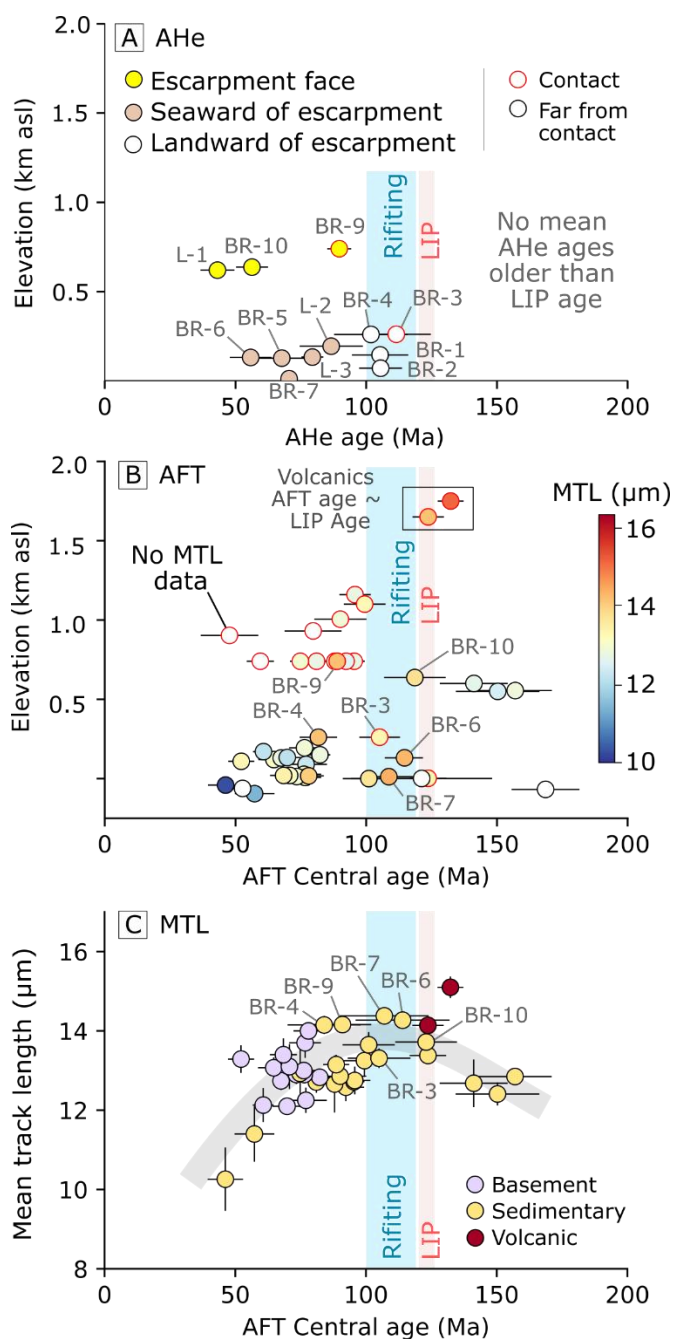


Figure 4 – AHe and AFT results according to elevation. A) Mean AHe age, color-coded by location. B) AFT central ages color-coded by MTL. C) AFT central ages vs. MTL results (“boomerang” plot), color-coded by lithology. B and C include data from Gallagher et al. (1994), Karl et al. (2013), Krob et al. (2019), and Bicca et al. (2020).

4.2 Thermal history modelling

Collectively, all joint (AHe and AFT) models (Figs. 5D-G) are consistent with a discrete temperature increase of $\sim 70 - 90$ °C at the time of the LIP emplacement ca. 133 Ma (Fig. 5B). Following this temperature increase, modeling results reveal an accelerated cooling phase from 120 – 90 Ma ($1 - 9$ °C Myr⁻¹; Fig. 5C). This cooling phase is followed by slow, protracted cooling during the post-rift period in the Late Cretaceous throughout the Cenozoic. Overall, post-rifting (100 – 66 Ma) cooling rates are < 3 °C Myr⁻¹, while Cenozoic rates indicate near-surface temperatures with maximum cooling rates of < 1 °C Myr⁻¹ (Fig. 5C).

5 DISCUSSION

5.1 Heating events

In the study area, single-grain AHe cooling ages range from 17 to 254 Ma, with $\sim 95\%$ of all dated grains younger than the Paraná-Etendeka LIP emplacement (Fig. 3B, SI5). In contrast, AFT central ages range from 46 to 222 Ma, with 89% of central ages postdating the LIP (Fig. 3C, SI5) (Gallagher et al., 1994; Karl et al., 2013; Krob et al., 2019; Bicca et al., 2020). Notably, samples collected far from lava contact zones also yield young cooling ages, indicating that the observed age reset is not restricted to localized contact-related thermal effects. This indicates that the high thermal flux associated with the LIP, likely in combination with significant overburden, was sufficient to fully reset nearly all AHe dates in the study site (e.g., Hueck et al., 2018). However, the AFT system was only partially reset, consistent with previous results from sedimentary samples analyzed by Gallagher et al. (1994), which

suggest a limited sensitivity of AFT to post-LIP thermal events. This observation is supported by the notable dispersion observed in AFT dates ([Table 2](#)).

All AFT central ages are younger than the depositional age of the Rio do Rastro Fm. (~250 Ma, SI5), therefore matching the Gondwana I subsidence cycle of the Paraná Basin ([Canile et al., 2016](#)). Collectively, these results suggest that thermal effects associated with both the Gondwana I depositional cycle (~190 Ma) and the later emplacement of the Serra Geral Group/Paraná-Etendeka LIP (~133 Ma) played an important role in annealing and resetting apatite ages in the Aparados da Serra region. These observations are supported by inverse thermal history modeling results, which are consistent with a notable temperature increase at ~133 Ma in all modelled samples ([Fig. 5](#)). Therefore, our analyses support the hypothesis of widespread heating/burial associated with the emplacement of the Paraná-Etendeka LIP ([Gallagher et al., 1994](#); [Hueck et al., 2018](#)). Based on inverse thermal history models, we observe cooling paths compatible with a minimum temperature increase of ~ 65 – 95 °C for joint (AFT and AHe) models, equivalent to a minimum overburden of ~ 1.6 – 2.3 km of rock material if we consider a geothermal gradient between 30 and 40 °C km⁻¹ ([Fig. 5B](#)). These values agree with overburden estimates obtained by previous studies in the Aparados da Serra (ca. 2.5 km; [Gallagher et al., 1994](#); [Karl et al., 2013](#); [Hueck et al., 2019](#); [Krob et al., 2019](#); [Bicca et al., 2020](#)).

Thermochronology results from other regions affected by LIPs support the discrete heating pattern observed in our study area. For instance, [Colleps et al. \(2021\)](#) demonstrated that the Deccan Traps experienced a distinct thermal pulse, likely reflecting a significant

thermal overprint caused by elevated regional heat flow, increased overburden, or a combination of both. Similarly, the emplacement of extensive dike swarms, sills, and thick volcanic flows, features commonly associated with LIPs and rifted margins, are suggested to substantially increase local geothermal gradients (Nyblade & Sleep, 2003; Krob et al., 2020). Consequently, both spatially and temporally variable geothermal gradients are expected across regions affected by LIPs (e.g., Nyblade & Sleep, 2003). Therefore, it is important to note that the interpretations presented in this study do not fully account for these heterogeneities, which could influence the inferred thermal histories.

5.2 Exhumation rates

Joint inverse thermal history models suggest protracted exhumation histories in the Aparados da Serra coastal plain since rifting ca. 120 – 100 Ma (Fig. 5). For geothermal gradients of 30 – 40 °C km⁻¹, modeled samples indicate exhumation rates of ~ 50 m Myr⁻¹ for the Late Cretaceous, although peaks of accelerated exhumation between 100 – 300 m Myr⁻¹ are observed in two samples at ~ 110 Ma (BR-3 and BR-4, Fig. 6B). In the Cenozoic, all modeled samples reveal exhumation rates < 25 m Myr⁻¹ (Fig. 6B). For the coastal plain region (BR-6 and 7), modelled Cenozoic rates of < 20 m Myr⁻¹ are within the same order of magnitude as low-temperature thermochronology (AHe + AFT) results obtained by Karl et al. (2013) and Krob et al. (2019), who documented rates of ~ 12 m Myr⁻¹ and 23 – 68 m Myr⁻¹, respectively. Modelled Cenozoic rates are also comparable to short-term erosion rates obtained using terrestrial cosmogenic nuclides (TCNs) in escarpment-draining rivers from the Aparados da Serra (5 – 136 m Myr⁻¹; Haag et al., 2025a).

Samples collected landward of the escarpment (South group, samples BR-1 to 4) are considered to be potentially representative of plateau erosion rates. Modelled rates of these samples suggest an accelerated phase of exhumation up to 300 m Myr⁻¹ from ca. 115 – 95 Ma, followed by protracted, low exhumation rates of < 10 m Myr⁻¹ from 90 Ma to present (Fig. 6B). Based on their present-day elevation (> 600 m asl), samples collected along the escarpment face (North group, samples BR-9, 10 and L-1) are also considered as potentially representative of erosion rates in the plateau. Similar to BR-1 to 4, north group samples feature an accelerated exhumation phase up to 40 m Myr⁻¹ from 105 – 90 Ma (Fig. 6B). An elevation profile using mean AHe ages (samples BR-9, BR-10 from this study and L-1 from Krob et al., 2019) indicates exhumation rates of the plateau of only 2.6 m Myr⁻¹ from 90 – 40 Ma (Fig. 2D). In contrast, modelled rates for the same period using the same samples indicate slightly higher exhumation rates of 16 – 22 m Myr⁻¹ (Fig. 6B). These rates are in agreement with TCN-derived erosion rates of 6 m Myr⁻¹ for plateau-draining rivers in the study area (Haag et al., 2025a). They also match the expected short-term erosion rates of other EPMS plateaus, including south and western Africa (Makubela et al., 2021), eastern Australia (Codilean et al., 2021), western Madagascar (Wang and Willett, 2021; Brosens et al., 2023), and western India (Mandal et al., 2015), where TCN rates range from 2.7 to 47 m Myr⁻¹.

Collectively, although quantifying how erosion rates varied across the entire Cenozoic remains challenging, our results are compatible with remarkably low erosion rates in the Aparados da Serra throughout the Cenozoic. The persistence of such low denudation underscores the long-term stability of the volcanic plateau and associated escarpment.

Building on these results, the following section explores the potential mechanisms that may account for the long-term uplift of the study area.

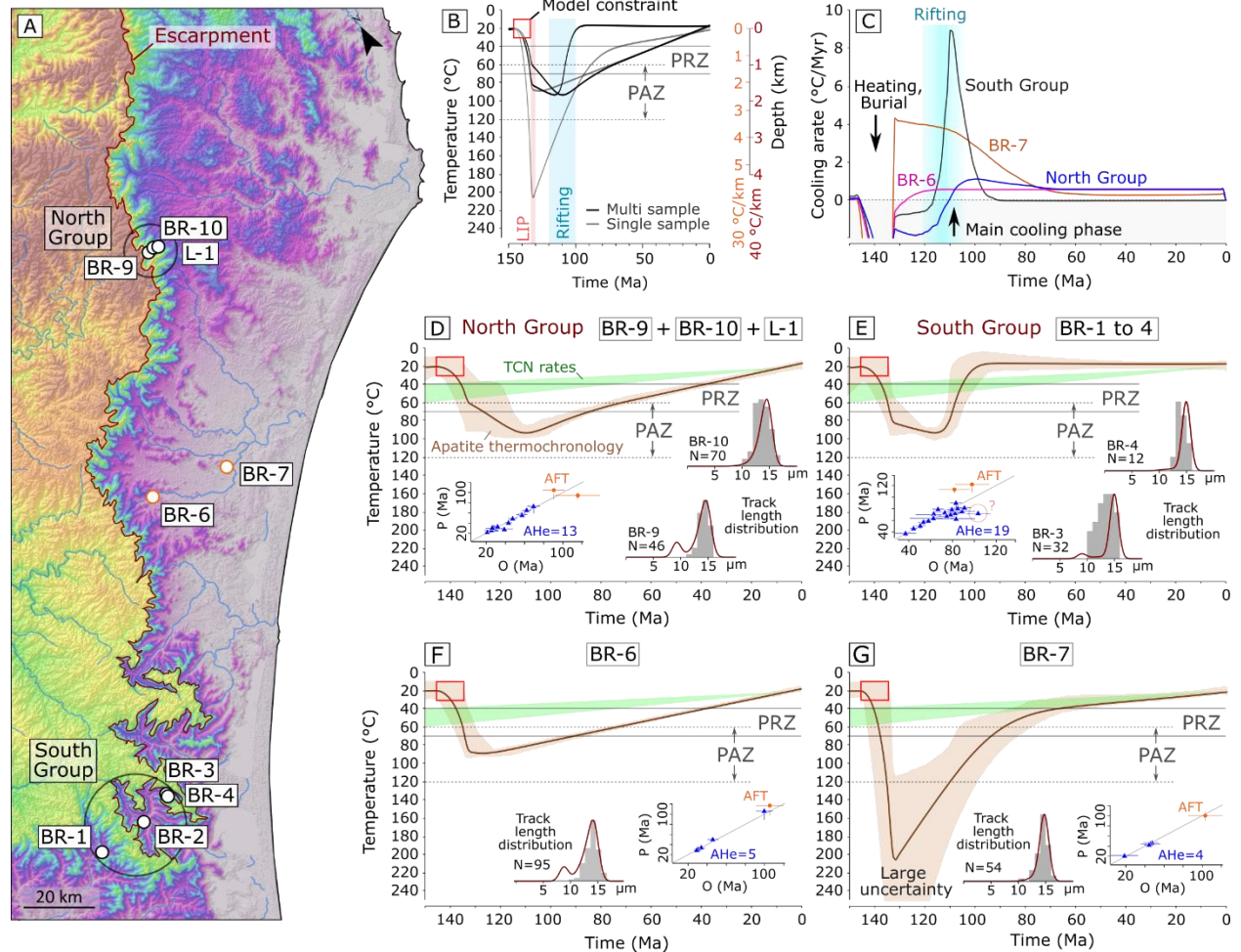


Figure 5 – Inverse thermal history modeling results for samples from the Aparados da Serra escarpment. A) Overview of sampling sites. B) Summary of cooling paths for modelled samples and expected burial depths for 30 and 40 °C km⁻¹ geothermal gradients. C) Summary of cooling rates calculated based on modelled cooling paths presented in (B). D-G) Model results: The brown line in each panel represents the expected thermal history model, while the shaded brown area denotes the 95% confidence interval. Green areas show projected terrestrial cosmogenic nuclide (TCN) erosion rates measured on the Aparados da Serra Plateau (Haag et al., 2025a). Note that TCN rates integrate over short timescales of <1 Myr and are not representative beyond this interval; accordingly, TCN rates are projected further back in time for illustrative purposes only.

Measured track length distributions are shown as grey histograms, with predicted track length distributions in maroon. Observed (O) and predicted (P) AFT central ages are shown as orange circles (●), as single-grain AHe ages are shown as blue triangles (▲).

5.3 Timing of uplift and potential mechanisms

Thermal history model results suggest relatively low and uniform exhumation rates across the Aparados da Serra since rifting (Fig. 5C, 6B). These findings are supported by previous studies conducted in the study region (Gallagher et al., 1994; Karl et al., 2013; Krob et al., 2019; Bicca et al., 2020), which document protracted erosion from the Late Cretaceous to the present. Furthermore, the consistency in erosion and exhumation rates across multiple techniques with contrasting temporal resolutions (AFT, AHe, and TCNs; Haag et al., 2025a) further supports the interpretation of slow, protracted denudation throughout the Cenozoic. Combined, these observations indicate that the timing of uplift was likely contemporaneous with continental rifting and/or LIP emplacement (Fig. 6A, B), and that the Aparados da Serra has since undergone protracted topographic decay (e.g., Nielsen et al., 2009; Jess et al., 2019) rather than recent tectonic rejuvenation (e.g., Japsen et al., 2012). Our results, therefore, do not fit the cyclic uplift model suggested by Japsen et al. (2012) for the evolution of EPMs.

Curiously, we observe no apparent relationship between modeled exhumation rates, climate records (Veizer et al., 1999; Mills et al., 2019), sediment flux into the Pelotas Basin (Contreras et al., 2010; Rohais et al., 2021), mid-Atlantic ridge spreading rates (Clark, 2018), and Andean convergence rates (Maloney et al. 2013; Horton, 2018) (Fig. 6B-F). This decoupling suggests that the influence of far-field stresses, whether from the Andean

orogeny (e.g., [Van Ranst et al., 2020](#)) or the Atlantic mid-ocean ridge, on exhumation in the Aparados da Serra region has been limited, or possibly too subtle to detect with low-temperature thermochronology (e.g., [Contreras et al., 2010](#); [Rohais et al., 2021](#)). Therefore, even though sedimentary fluxes have been used to infer uplift and exhumation events in various passive margin settings (e.g., [Baby et al., 2018](#)), here we also observe no relationship between tectonics and sedimentary input into the Pelotas Basin. Additionally, major unconformities are primarily associated with eustatic sea-level fluctuations ([Contreras et al., 2010](#)), rather than tectonic activity.

Based on the comprehensive chart presented in Fig. 6, the Paraná-Etendeka LIP and subsequent continental rifting were likely the last major events capable of influencing low-temperature thermochronology systems in the Aparados da Serra. Recent geodynamic models further support the interpretation that long-lived topography along rifted margins may reflect rift-related lithospheric processes rather than post-rift tectonic rejuvenation. Using global numerical models, Gernon et al. (2024) demonstrate that coupled evolution of craton interiors during continental break-up create persistent buoyancy contrasts that stabilize elevated topography for hundreds of millions of years. As a result, rift-adjacent margins may retain high elevations long after breakup, even in the absence of significant post-rift deformation or dynamic topographic forcing (Gernon et al., 2024). The Aparados da Serra escarpment is consistent with this model, as its elevated topography and protracted low exhumation rates may be explained by rift- and LIP-related lithospheric modification.

Particularly relevant to the establishment of permanent uplift, extensive evidence of magmatic underplating in southeast Brazil suggests that this process may have played a key role in generating elevated topography (Mariani et al., 2013; Bernardes et al., 2023). Therefore, the Cenozoic evolution of the Aparados da Serra greatly contrasts with other parts of the Brazilian EPM, where tectonic reactivation is locally present (Riccomini et al., 1989; Cogné et al., 2012; Sacek et al., 2012; Fonte-Boa et al., 2022; Fonseca et al., 2023). Fonte-Boa et al. (2022) demonstrated that the Brazilian EPM exhibits remarkable diversity and therefore should not be treated as a single, uniform margin. Across the margin, important differences in crustal rheology, inherited structures, and the spatio-temporal distribution of post-breakup magmatism play a key role in shaping its evolution. Accordingly, while the northern segment of the margin has been interpreted to reflect the influence of crustal rheology and post-breakup tectonic reactivation (Sacek et al., 2012), surface geology and structural mapping indicate that the southern segment has not been significantly affected by Cenozoic rifting or widespread post-breakup extensional deformation. This fundamental difference suggests that variations in crustal rheology and tectonic reactivation played a much more limited role in shaping the southern margin, favoring long-term topographic stability rather than Cenozoic rejuvenation.

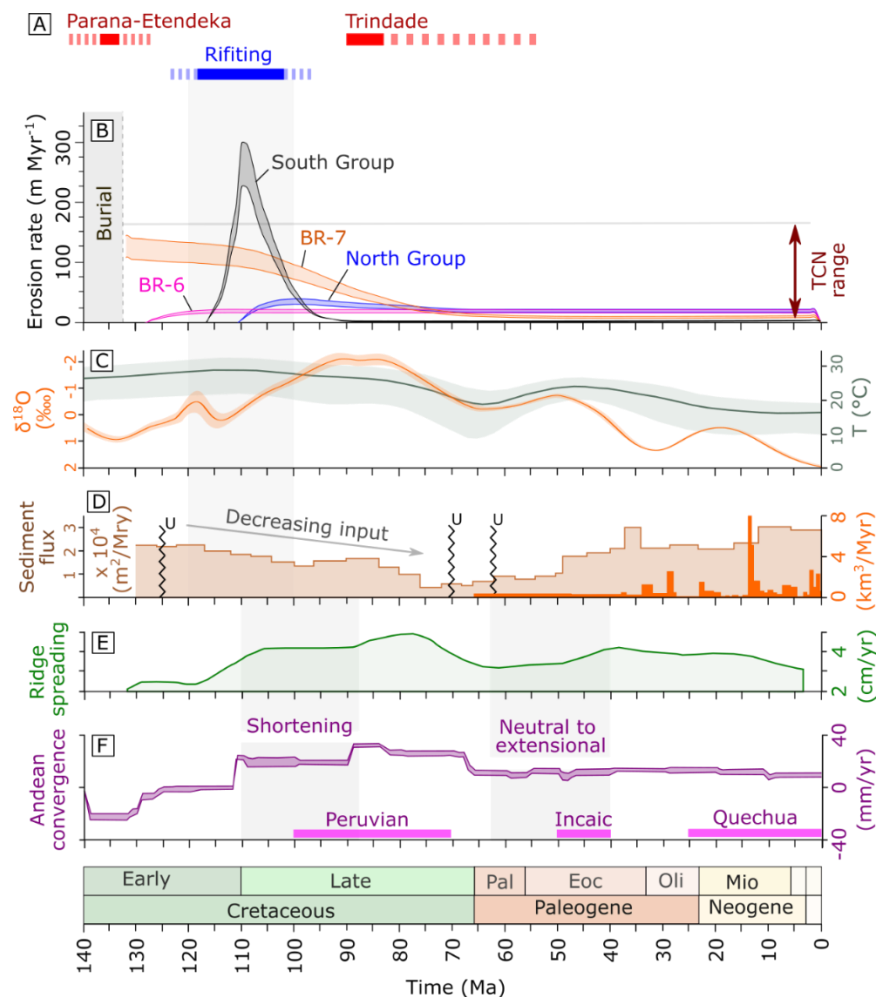


Figure 6 – Apatite low-temperature thermochronology exhumation rates for the Aparados da Serra compared to stratigraphic records and tectonic events in South America. A) Major tectono-magmatic events in eastern South America (Thompson et al., 1998; Gibson et al., 1999; Maia et al., 2021; Gomes and Vasconcelos, 2021 and references therein). B) Exhumation rates calculated for geothermal gradients 30 – 40 °C km⁻¹. C) Global climate record (Veizer et al., 1999 for δ¹⁸O record (in parts per thousand = ‰) and Mills et al., 2019 for surface temperature). D) Sediment flux (light orange) from offshore sedimentary record of the *Pelotas* Basin (depocenter of the study area), including calibrated sedimentary input and erosional shelf unconformities (U) (light brown, Contreras et al., 2010) and high-resolution Cenozoic data (dark orange, Rohais et al., 2021). E) South Atlantic mid-ocean ridge spreading rates (green curve, Clark, 2018). F) Andean convergence velocity (purple curve, Maloney et al. 2013; Horton, 2018) and phases (dark pink bars, Cobbold et al., 2001).

5.4 Geomorphologic evolution

In addition to the timing and origin of topography along the study area, the spatial distribution of AFT and AHe ages, and their modelled rates, allow us to evaluate the long-term geomorphologic evolution of the southern Brazilian EPM. While the denudation of EPMs can evolve via several pathways (Gallagher et al., 1998), two end-member scenarios are generally recognized: (i) escarpment retreat and (ii) plateau degradation (Brown et al., 2002; van der Beek et al., 2002; Braun and van der Beek, 2004). The escarpment retreat model suggests a drainage divide that coincides with the rift axis and progressively migrates landward by escarpment back cutting (Fig. 7A) (van der Beek et al., 2002). In contrast, the plateau degradation model assumes a drainage divide located several tens of kilometers landward of the rift axis; in this scenario, a fast period of erosion is focused on the region between the divide and the rift axis (Fig. 7B) (van der Beek et al., 2002).

Geodynamic conditions potentially favor the use of AHe for discriminating between these two scenarios in the study area. Low to moderate values of effective elastic thickness of the lithosphere (~ 10 – 40 km; Tassara et al., 2007), high geothermal gradients (30 – 35°C Km⁻¹, but likely higher in the past; Vieira and Hamza, 2019), and sufficient inland migration of the escarpment (migration distance ≥ characteristic wavelength of flexural deflection, which ranges from 30 – 80 km in the study area; Haag et al., 2025b) all point to a likely flexural response to erosion and therefore a detectable AHe trend along the coastal plain (Braun and van der Beek, 2004). However, the moderate elevation of the Aparados da Serra escarpment

(1–1.6 km asl) places it at the lower limit for detecting escarpment retreat using AHe data (Braun and van der Beek, 2004).

We compare our AHe data with the expected distribution of AHe dates for the escarpment retreat and the plateau degradation denudation scenarios obtained by Braun and van der Beek (2004) using numerical models (Fig. 7C, D). The models of Braun and van der Beek (2004) simulate the long-term evolution of a ~100 Ma-old elevated passive margin (~1 km relief) under relatively high geothermal gradients, assuming a weak lithosphere with an effective elastic thickness of ~10 km. These conditions are broadly similar with those observed in the Aparados da Serra. Accordingly, for this comparison, sample locations were normalized to the distance between the inferred rift axis and the escarpment base, and all AHe ages were normalized to the timing of rifting: 100 Ma in the models of Braun and van der Beek (2004) and ~110 Ma for the Aparados da Serra (Stica et al., 2014). In this framework, we treat the offshore hinge line as the most likely location of the paleo-rift axis (Contreras et al., 2010; Stica et al., 2014).

This comparison reveals that AHe ages from the coastal region of the Aparados da Serra are significantly younger than those predicted in the plateau degradation scenario (Fig. 7C). In this geomorphic evolution pathway, AHe dates on the coastal plain are expected to be 25 – 50% older than rifting (Fig. 7D; Braun and van der Beek, 2004). This is not observed in the AHe dates reported in the Aparados da Serra, which are generally 25 – 70% younger than the rifting. Accordingly, the spatial distribution and overall range of AHe ages appears to favor the escarpment retreat hypothesis, characterized by (i) a progressive decrease of AHe ages

toward the escarpment bottom and (ii) ages that are typically younger than rifting (Fig. 7D) (Braun and van der Beek, 2004).

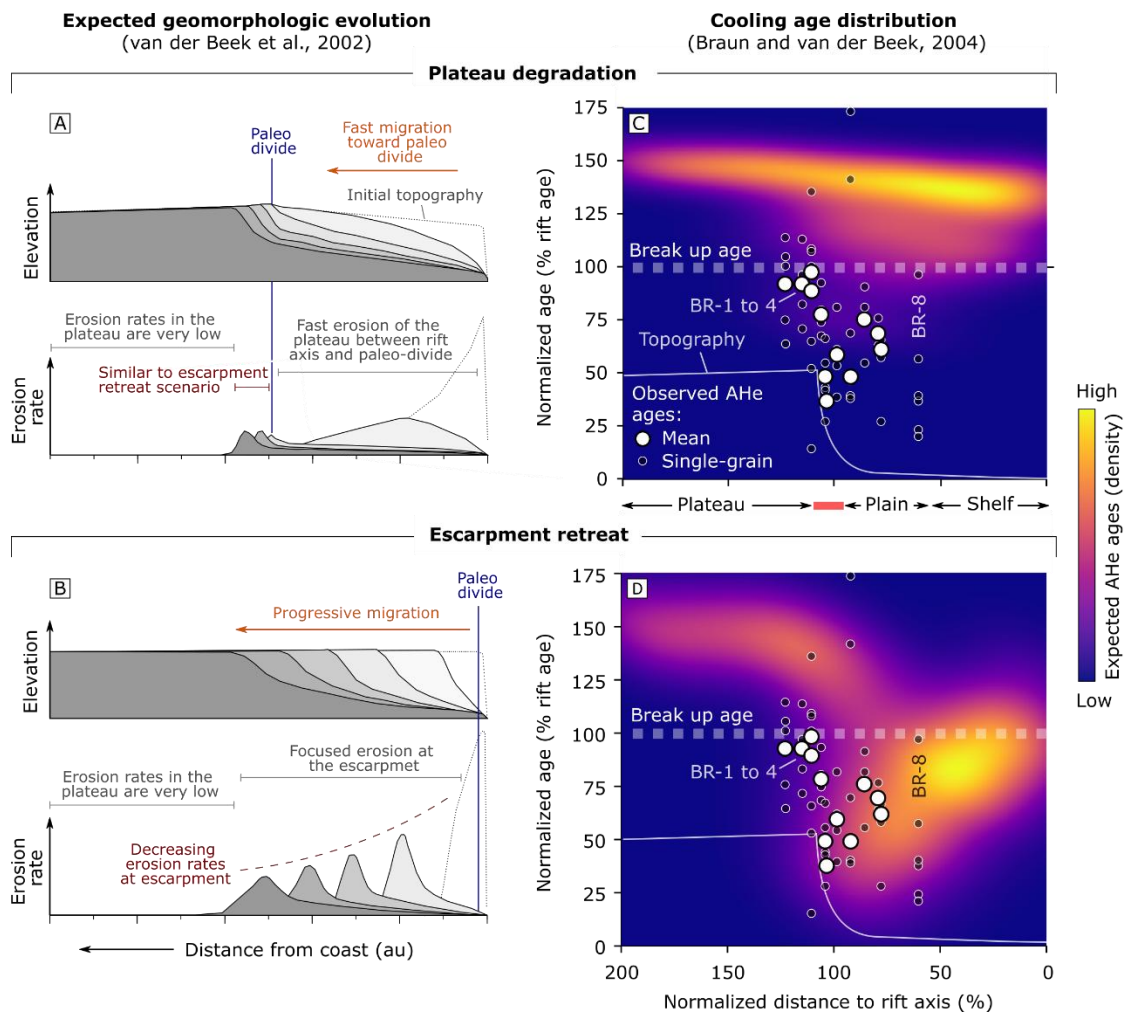


Figure 7 – Exhumation patterns expected for the (A, C) plateau degradation and (B, D) escarpment retreat scenarios with the respective locus of erosion since rifting. The geomorphologic evolution (A,C) depicts the modeling results of van der Beek (2002), while the expected distribution of AHe ages (B,D) is based on Braun and van der Beek (2004) results for . Elevation and erosion rates in the left-side plot are arbitrary.

Additionally, despite the overall spatial pattern and age distribution apparently supporting the escarpment retreat scenario, inverse thermal history models for samples collected along the coastal plain (Fig. 5; BR-6 and BR-7) do not exhibit a distinct, accelerated

phase of exhumation expected in response to an erosional wave due to escarpment migration ([Fig. 7B](#)). Instead, the modeled samples indicate relatively steady and prolonged cooling, compatible with gradual plateau denudation ([Fig. 5](#)). In this context, the lack of an exhumation pulse may imply that the coastal plain experienced subdued erosional dynamics, or that any signal of rapid retreat has been thermally overprinted or spatially averaged out. Alternatively, it may also indicate that the exhumation caused by the migrating escarpment was not significant enough to result in a detectable signal in the thermal models.

Therefore, the present dataset does not allow us to confidently differentiate between escarpment retreat and plateau degradation as the dominant post-rift erosional process in the Aparados da Serra. Although the spatial pattern of AHe ages appears consistent with an escarpment retreat model, quantifying retreat rates remains challenging with the available number of samples. For an effective elastic thickness ranging between ~10 and 40 km ([Tassara et al., 2007](#)), the minimum AHe ages are expected to be older than escarpment stabilization times ([Braun and van der Beek, 2004](#)). These results highlight that effective elastic thickness can exert a first-order control on EPM evolution (e.g., [Braun et al., 2013](#)) and complicate efforts to infer exhumation rates from thermochronologic data in these settings. Therefore, minimum observed AHe ages of approximately ~55 Ma only provide a first-order estimate for the timing of escarpment stabilization in the Aparados da Serra.

6 CONCLUSIONS

In this study we present novel AHe and AFT data for the southern end of the Brazilian elevated passive margin. Based on cooling ages, geological, and thermal history model observations, we identify that:

- The Aparados da Serra is marked by monotonic, slow cooling rates typically < 50 m Myr⁻¹. These rates are compatible with recently obtained, short term, TCN erosion rates (Haag et al., 2025a).
- Thermal histories show no evidence of recent accelerated cooling episodes, implying either an absent or undetectable Cenozoic uplift in the study area. Therefore, the elevated topography observed in the Aparados da Serra EPM was likely achieved during rifting at ca. 120 – 100 Ma.
- The spatial distribution of AHe dates, and their ages, appears to favour the escarpment retreat hypothesis for the geomorphic evolution of the Aparados da Serra. This hypothesis, however, is not supported by inverse models, which show not particular erosional wave.

ACKNOWLEDGMENTS & FUNDING

We thank Joshua Wolpert for his assistance in the field during sample collection, and Kerry Gallagher and David Peate for sharing their sampling strategies and site locations in southeast Brazil. We also thank Mauricio Parra and two anonymous reviewers for their

This article has been peer-reviewed and is now freely available (open access) at *Tectonophysics*: <https://doi.org/10.1016/j.tecto.2026.231100>.

constructive comments, which helped improve the clarity and quality of the manuscript.

This work was partially funded with an NSERC Discovery Grant awarded to L.M.S.

REFERENCES

Baby, G., Guillocheau, F., Morin, J., Ressouche, J., Robin, C., Broucke, O., Dall'Asta, M., 2018. Post-rift stratigraphic evolution of the Atlantic margin of Namibia and South Africa: Implications for the vertical movements of the margin and the uplift history of the South African Plateau. *Marine and Petroleum Geology*. <https://doi.org/10.1016/j.marpetgeo.2018.06.030>

Bernardes, R.B., Soares, J.E.P., Lima, M.V.A.G. de, Fuck, R.A., Viana, A.R., 2023. Cretaceous magmatic underplating and delamination beneath continental SE Brazil and their tectonic implications: Evidence from the PABBRISE wide-angle reflection and refraction seismic profile. *Tectonophysics*. <https://doi.org/10.1016/j.tecto.2023.229856>

Bertolini, G., Marques, J.C., Hartley, A.J., Da-Rosa, A.A.S., Scherer, C.M.S., Basei, M.A.S., Frantz, J.C., 2020. Controls on Early Cretaceous desert sediment provenance in south-west Gondwana, Botucatu Formation (Brazil and Uruguay). *Sedimentology*. <https://doi.org/10.1111/sed.12715>

Bicca, M.M., Kalkreuth, W., da Silva, T.F., de Oliveira, C.H.E., Genezini, F.A., 2020. Thermal and depositional history of Early-Permian Rio Bonito Formation of southern Paraná Basin – Brazil. *International Journal of Coal Geology*. <https://doi.org/10.1016/j.coal.2020.103554>

Braun, J., 2018. A review of numerical modeling studies of passive margin escarpments leading to a new analytical expression for the rate of escarpment migration velocity. *Gondwana Research*. <https://doi.org/10.1016/j.gr.2017.04.012>

This article has been peer-reviewed and is now freely available (open access) at *Tectonophysics*: <https://doi.org/10.1016/j.tecto.2026.231100>.

Braun, J., van der Beek, P., 2004. Evolution of passive margin escarpments: What can we learn from low-temperature thermochronology? *J. Geophys. Res.* <https://doi.org/10.1029/2004jf000147>

Braun, J., Deschamps, F., Rouby, D., Dauteuil, O., 2013. Flexure of the lithosphere and the geodynamical evolution of non-cylindrical rifted passive margins: Results from a numerical model incorporating variable elastic thickness, surface processes and 3D thermal subsidence. *Tectonophysics* 604, 72–82. <https://doi.org/10.1016/j.tecto.2012.09.033>

Brosens, L., Cox, R., Campforts, B., Jacobs, L., Vanacker, V., Bierman, P., Razanamahandry, V.F., Rakotondrazafy, A.F.M., Razafimbelo, T., Rafolisy, T., Govers, G., 2023. The slow downwearing of Madagascar: Inferring patterns and controls on long-term basin-averaged erosion rates from in situ ^{10}Be at the catchment and regional level. *Earth Surf Processes Landf.* <https://doi.org/10.1002/esp.5586>

Brown, R.W., Summerfield, M.A., Gleadow, A.J.W., 2002. Denudational history along a transect across the Drakensberg Escarpment of southern Africa derived from apatite fission track thermochronology. *J. Geophys. Res.* <https://doi.org/10.1029/2001jb000745>

Canile, F.M., Babinski, M., Rocha-Campos, A.C., 2016. Evolution of the Carboniferous-Early Cretaceous units of Paraná Basin from provenance studies based on U-Pb, Hf and O isotopes from detrital zircons. *Gondwana Research.* <https://doi.org/10.1016/j.gr.2016.08.008>

Chaves, C., Ussami, N., Ritsema, J., 2016. Density and P-wave velocity structure beneath the Paraná Magmatic Province: Refertilization of an ancient lithospheric mantle. *Geochem. Geophys. Geosyst.* <https://doi.org/10.1002/2016gc006369>

Clark, S.R., 2018. Uncertainty in the breakup, spreading history, and velocity variations of Gondwana. *Gondwana Research.* <https://doi.org/10.1016/j.gr.2017.04.029>

This article has been peer-reviewed and is now freely available (open access) at *Tectonophysics*:
<https://doi.org/10.1016/j.tecto.2026.231100>.

Cobbold, P.R., Rossello, E.A., Roperch, P., Arriagada, C., Gómez, L.A., Lima, C., 2007. Distribution, timing, and causes of Andean deformation across South America. SP.

<https://doi.org/10.1144/gsl.sp.2007.272.01.174>

Codilean, A.T., Fülöp, R.-H., Munack, H., Wilcken, K.M., Cohen, T.J., Rood, D.H., Fink, D., Bartley, R., Croke, J., Fifield, L.K., 2021. Controls on denudation along the East Australian continental margin.

Earth-Science Reviews. <https://doi.org/10.1016/j.earscirev.2021.103543>

Cogné, N., Gallagher, K., Cobbold, P.R., 2011. Post-rift reactivation of the onshore margin of southeast Brazil: Evidence from apatite (U–Th)/He and fission-track data. Earth and Planetary

Science Letters. <https://doi.org/10.1016/j.epsl.2011.06.025>

Cogné, N., Gallagher, K., Cobbold, P.R., Riccomini, C., Gautheron, C., 2012. Post-breakup tectonics in southeast Brazil from thermochronological data and combined inverse-forward thermal history

modeling. J. Geophys. Res. <https://doi.org/10.1029/2012jb009340>

Colleps, C.L., McKenzie, N.R., Guenthner, W.R., Sharma, M., Gibson, T.M., Stockli, D.F., 2021.

Apatite (U–Th)/He thermochronometric constraints on the northern extent of the Deccan large igneous province. Earth and Planetary Science Letters 571, 117087.

<https://doi.org/10.1016/j.epsl.2021.117087>

Contreras, J., Zühlke, R., Bowman, S., Bechstädt, T., 2010. Seismic stratigraphy and subsidence analysis of the southern Brazilian margin (Campos, Santos and Pelotas basins). Marine and

Petroleum Geology. <https://doi.org/10.1016/j.marpetgeo.2010.06.007>

Danišík, M., Kirkland, C.L., 2023. Thermochronometry constraints on south West Greenland

passive continental margin development. Commun Earth Environ. [https://doi.org/10.1038/s43247-](https://doi.org/10.1038/s43247-023-00786-6)

[023-00786-6](https://doi.org/10.1038/s43247-023-00786-6)

This article has been peer-reviewed and is now freely available (open access) at *Tectonophysics*:
<https://doi.org/10.1016/j.tecto.2026.231100>.

Donelick, R.A., 2005. Apatite Fission-Track Analysis. *Reviews in Mineralogy and Geochemistry*.
<https://doi.org/10.2138/rmg.2005.58.3>

Evans, N.J., Byrne, J.P., Keegan, J.T., Dotter, L.E., 2005. Determination of Uranium and Thorium in Zircon, Apatite, and Fluorite: Application to Laser (U-Th)/He Thermochronology. *J Anal Chem*.
<https://doi.org/10.1007/s10809-005-0260-1>

Flowers, R.M., Ketcham, R.A., Shuster, D.L., Farley, K.A., 2009. Apatite (U–Th)/He thermochronometry using a radiation damage accumulation and annealing model. *Geochimica et Cosmochimica Acta*. <https://doi.org/10.1016/j.gca.2009.01.015>

Fonseca, A., Novo, T., Fonte-Boa, T., Kuchenbecker, M., Fragoso, D.G.C., Peifer, D., Pedrosa-Soares, A.C., De Grave, J., 2023. Control of inherited structural fabric on the development and exhumation of passive margins – Insights from the Araçuaí Orogen (Brazil). *Geoscience Frontiers* 14, 101628.
<https://doi.org/10.1016/j.gsf.2023.101628>

Fonte-Boa, T.M.R., Peifer, D., Fonseca, A., Novo, T.A., 2022. The southeast Brazilian rifted continental margin is not a single, continuous upwarp: Variations in morphology and denudation patterns along the continental drainage divide. *Earth-Science Reviews*.
<https://doi.org/10.1016/j.earscirev.2022.104091>

Fraser, K.I., Enkelmann, E., Jess, S., Gilbert, H., Grieco, R., 2021. Resolving the Cenozoic History of Rock Exhumation Along the Central Rocky Mountain Trench Using Apatite Low-Temperature Thermochronology. *Tectonics*. <https://doi.org/10.1029/2021tc006847>

Gallagher, K., 2012. Transdimensional inverse thermal history modeling for quantitative thermochronology. *J. Geophys. Res.* <https://doi.org/10.1029/2011jb008825>

This article has been peer-reviewed and is now freely available (open access) at *Tectonophysics*:
<https://doi.org/10.1016/j.tecto.2026.231100>.

Gallagher, K., Brown, R., Johnson, C., 1998. Fission Track Analysis And Its Applications To Geological Problems. *Annu. Rev. Earth Planet. Sci.* <https://doi.org/10.1146/annurev.earth.26.1.519>

Gallagher, K., Hawkesworth, C.J., Mantovani, M.S.M., 1994. The denudation history of the onshore continental margin of SE Brazil inferred from apatite fission track data. *J. Geophys. Res.* <https://doi.org/10.1029/94jb00661>

Gautheron, C., Tassan-Got, L., Barbarand, J., Pagel, M., 2009. Effect of alpha-damage annealing on apatite (U–Th)/He thermochronology. *Chemical Geology* 266, 157–170.
<https://doi.org/10.1016/j.chemgeo.2009.06.001>

Gautheron, C., Tassan-Got, L., Ketcham, R.A., Dobson, K.J., 2012. Accounting for long alpha-particle stopping distances in (U–Th–Sm)/He geochronology: 3D modeling of diffusion, zoning, implantation, and abrasion. *Geochimica et Cosmochimica Acta.* <https://doi.org/10.1016/j.gca.2012.08.016>

Gerin, C., Gautheron, C., Oliviero, E., Bachelet, C., Mbongo Djimbi, D., Seydoux-Guillaume, A.-M., Tassan-Got, L., Sarda, P., Roques, J., Garrido, F., 2017. Influence of vacancy damage on He diffusion in apatite, investigated at atomic to mineralogical scales. *Geochimica et Cosmochimica Acta* 197, 87–103. <https://doi.org/10.1016/j.gca.2016.10.018>

Gernon, T.M., Hincks, T.K., Brune, S., Braun, J., Jones, S.M., Keir, D., Cunningham, A., Glerum, A., 2024. Coevolution of craton margins and interiors during continental break-up. *Nature.* <https://doi.org/10.1038/s41586-024-07717-1>

Gezatt, J.N., Macdonald, D.I.M., Stephenson, R., Jelinek, A.R., Carter, A., 2021. South Atlantic passive margin evolution: A thermochronology case study from the Rio de Janeiro-Três Rios section, SE Brazil. *Journal of South American Earth Sciences.* <https://doi.org/10.1016/j.jsames.2020.103051>

This article has been peer-reviewed and is now freely available (open access) at *Tectonophysics*:
<https://doi.org/10.1016/j.tecto.2026.231100>.

Gibson, S.A., Thompson, R.N., Leonardos, O.H., Dickin, A.P., Mitchell, J.G., 1999. The limited extent of plume-lithosphere interactions during continental flood-basalt genesis: geochemical evidence from Cretaceous magmatism in southern Brazil. *Contributions to Mineralogy and Petrology*.

<https://doi.org/10.1007/s004100050588>

Gomes, A.S., Vasconcelos, P.M., 2021. Geochronology of the Paraná-Etendeka large igneous province. *Earth-Science Reviews*. <https://doi.org/10.1016/j.earscirev.2021.103716>

Gomes, M.C.V., Vieira, B.C., Salgado, A.A.R., Braucher, R., 2022. Debris flow and long-term denudation rates in a tropical passive margin escarpment in South America. *Geomorphology*.

<https://doi.org/10.1016/j.geomorph.2022.108333>

Gonzalez, V.S., Bierman, P.R., Fernandes, N.F., Rood, D.H., 2016. Long-term background denudation rates of southern and southeastern Brazilian watersheds estimated with cosmogenic ^{10}Be .

Geomorphology. <https://doi.org/10.1016/j.geomorph.2016.05.024>

Green, P., Duddy, I., Japsen, P., 2022. Episodic kilometre-scale burial and exhumation and the importance of missing section. *Earth-Science Reviews*.

<https://doi.org/10.1016/j.earscirev.2022.104226>

Haag, M.B., Schoenbohm, L.M., Wolpert, J., Jess, S., Bierman, P., Corbett, L., Sommer, C.A., Endrizzi, G., 2025. Rock strength controls erosion in tectonically dead landscapes. *Sci. Adv.*

<https://doi.org/10.1126/sciadv.adr2610>

Härtel, B., Jonckheere, R., Krause, J., Ratschbacher, L., 2022. Spurious age-eU associations in thermochronological data. *Earth and Planetary Science Letters* 599, 117870.

<https://doi.org/10.1016/j.epsl.2022.117870>

This article has been peer-reviewed and is now freely available (open access) at *Tectonophysics*:
<https://doi.org/10.1016/j.tecto.2026.231100>.

Hasebe, N., Barbarand, J., Jarvis, K., Carter, A., Hurford, A.J., 2004. Apatite fission-track
chronometry using laser ablation ICP-MS. *Chemical Geology*.

<https://doi.org/10.1016/j.chemgeo.2004.01.007>

Hasebe, N., Tamura, A., Arai, S., 2013. Zeta equivalent fission-track dating using LA-ICP-MS and
examples with simultaneous U–Pb dating. *Island Arc*. <https://doi.org/10.1111/iar.12040>

Horton, B.K., 2018. Tectonic Regimes of the Central and Southern Andes: Responses to Variations
in Plate Coupling During Subduction. *Tectonics* 37, 402–429. <https://doi.org/10.1002/2017tc004624>

Hueck, M., Dunkl, I., Heller, B., Stipp Basei, M.A., Siegesmund, S., 2018. (U-Th)/He
Thermochronology and Zircon Radiation Damage in the South American Passive Margin: Thermal
Overprint of the Paraná LIP? *Tectonics*. <https://doi.org/10.1029/2018tc005041>

Hueck, M., Dunkl, I., Oriolo, S., Wemmer, K., Basei, M.A.S., Siegesmund, S., 2019. Comparing
contiguous high- and low-elevation continental margins: New (U-Th)/He constraints from South
Brazil and an integration of the thermochronological record of the southeastern passive margin of
South America. *Tectonophysics*. <https://doi.org/10.1016/j.tecto.2019.228222>

Japsen, P., Chalmers, J.A., Green, P.F., Bonow, J.M., 2012. Elevated, passive continental margins:
Not rift shoulders, but expressions of episodic, post-rift burial and exhumation. *Global and
Planetary Change*. <https://doi.org/10.1016/j.gloplacha.2011.05.004>

Jess, S., Stephenson, R., Roberts, D.H., Brown, R., 2019. Differential erosion of a Mesozoic rift flank:
Establishing the source of topography across Karrat, central West Greenland. *Geomorphology*.
<https://doi.org/10.1016/j.geomorph.2019.02.026>

This article has been peer-reviewed and is now freely available (open access) at *Tectonophysics*:
<https://doi.org/10.1016/j.tecto.2026.231100>.

Jess, S., Stephenson, R., Roberts, D.H., Brown, R., 2020. Reply to: Thermal history solutions from thermochronology must be governed by geological relationships: A comment on Jess et al. (2019). *Geomorphology*. <https://doi.org/10.1016/j.geomorph.2019.106971>

Karl, M., Glasmacher, U.A., Kollenz, S., Franco-Magalhaes, A.O.B., Stockli, D.F., Hackspacher, P.C., 2013. Evolution of the South Atlantic passive continental margin in southern Brazil derived from zircon and apatite (U–Th–Sm)/He and fission-track data. *Tectonophysics*.
<https://doi.org/10.1016/j.tecto.2013.06.017>

Ketcham, R.A., Gautheron, C., Tassan-Got, L., 2011. Accounting for long alpha-particle stopping distances in (U–Th–Sm)/He geochronology: Refinement of the baseline case. *Geochimica et Cosmochimica Acta*. <https://doi.org/10.1016/j.gca.2011.10.011>

Krob, F.C., Glasmacher, U.A., Bunge, H.-P., Friedrich, A.M., Hackspacher, P.C., 2020. Application of stratigraphic frameworks and thermochronological data on the Mesozoic SW Gondwana intraplate environment to retrieve the Paraná-Etendeka plume movement. *Gondwana Research*.
<https://doi.org/10.1016/j.gr.2020.02.010>

Krob, F.C., Glasmacher, U.A., Karl, M., Perner, M., Hackspacher, P.C., Stockli, D.F., 2019. Multi-chronometer thermochronological modelling of the Late Neoproterozoic to recent t-T-evolution of the SE coastal region of Brazil. *Journal of South American Earth Sciences*.
<https://doi.org/10.1016/j.jsames.2019.02.012>

Machado, J.P.S.L., Jelinek, A.R., Bicca, M.M., Stephenson, R., Genezini, F.A., 2019. West Gondwana orogenies and Pangaea break-up: thermotectonic effects on the southernmost Mantiqueira Province, Brazil. *JGS*. <https://doi.org/10.1144/jgs2019-018>

This article has been peer-reviewed and is now freely available (open access) at *Tectonophysics*:
<https://doi.org/10.1016/j.tecto.2026.231100>.

Machado, J.P.S.L., Jelinek, A.R., Stephenson, R., Gaucher, C., Müller Bicca, M., Chiglino, L., Genezini, F.A., 2020. Low-temperature thermochronology of the South Atlantic margin along Uruguay and its relation to tectonic events in West Gondwana. *Tectonophysics*.

<https://doi.org/10.1016/j.tecto.2020.228439>

Maia, T.M., dos Santos, A.C., Rocha-Júnior, E.R.V., Valeriano, C. de M., Mendes, J.C., Jeck, I.K., dos Santos, W.H., de Oliveira, A.L., Mohriak, W.U., 2021. First petrologic data for Vitória Seamount, Vitória-Trindade Ridge, South Atlantic: a contribution to the Trindade mantle plume evolution. *Journal of South American Earth Sciences*. <https://doi.org/10.1016/j.jsames.2021.103304>

Makhubela, T.V., Kramers, J.D., Konyana, S.M., van Niekerk, H.S., Winkler, S.R., 2021. Erosion rates and weathering timescales in the eastern Great Escarpment, South Africa. *Chemical Geology*.

<https://doi.org/10.1016/j.chemgeo.2021.120368>

Maloney, K.T., Clarke, G.L., Klepeis, K.A., Quevedo, L., 2013. The Late Jurassic to present evolution of the Andean margin: Drivers and the geological record. *Tectonics* 32, 1049–1065.

<https://doi.org/10.1002/tect.20067>

Mariani, P., Braitenberg, C., Ussami, N., 2013. Explaining the thick crust in Paraná basin, Brazil, with satellite GOCE gravity observations. *Journal of South American Earth Sciences*.

<https://doi.org/10.1016/j.jsames.2013.03.008>

McKay, R., Enkelmann, E., Hadlari, T., Matthews, W., Mouthereau, F., 2021. Cenozoic Exhumation History of the Eastern Margin of the Northern Canadian Cordillera. *Tectonics*.

<https://doi.org/10.1029/2020tc006582>

Milani, E.J., de Melo, J.H.G., de Souza, P.A., Fernandes, L.A., França, A.B., 2007. Bacia do Paraná *Bol. Geociencias Petrobras*, 15 (2), pp. 265-287.

This article has been peer-reviewed and is now freely available (open access) at *Tectonophysics*:
<https://doi.org/10.1016/j.tecto.2026.231100>.

Mills, B.J.W., Krause, A.J., Scotese, C.R., Hill, D.J., Shields, G.A., Lenton, T.M., 2019. Modelling the long-term carbon cycle, atmospheric CO₂, and Earth surface temperature from late Neoproterozoic to present day. *Gondwana Research*. <https://doi.org/10.1016/j.gr.2018.12.001>

Nielsen, S.B., Gallagher, K., Leighton, C., Balling, N., Svenningsen, L., Jacobsen, B.H., Thomsen, E., Nielsen, O.B., Heilmann-Clausen, C., Egholm, D.L., Summerfield, M.A., Clausen, O.R., Piotrowski, J.A., Thorsen, M.R., Huuse, M., Abrahamsen, N., King, C., Lykke-Andersen, H., 2009. The evolution of western Scandinavian topography: A review of Neogene uplift versus the ICE (isostasy–climate–erosion) hypothesis. *Journal of Geodynamics*. <https://doi.org/10.1016/j.jog.2008.09.001>

Nyblade, A.A., Sleep, N.H., 2003. Long lasting epeirogenic uplift from mantle plumes and the origin of the Southern African Plateau. *Geochem Geophys Geosyst* 4.
<https://doi.org/10.1029/2003gc000573>

Recanati, A., Gautheron, C., Barbarand, J., Missenard, Y., Pinna-Jamme, R., Tassan-Got, L., Carter, A., Douville, E., Bordier, L., Pagel, M., Gallagher, K., 2017. Helium trapping in apatite damage: Insights from (U-Th-Sm)/He dating of different granitoid lithologies. *Chemical Geology* 470, 116–131. <https://doi.org/10.1016/j.chemgeo.2017.09.002>

Riccomini, C., Peloggia, A.U.G., Saloni, J.C.L., Kohnke, M.W., Figueira, R.M., 1989. Neotectonic activity in the Serra do Mar rift system (southeastern Brazil). *Journal of South American Earth Sciences*. [https://doi.org/10.1016/0895-9811\(89\)90046-1](https://doi.org/10.1016/0895-9811(89)90046-1)

Rohais, S., Lovecchio, J.P., Abreu, V., Miguez, M., Paulin, S., 2021. High-resolution sedimentary budget quantification – Example from the Cenozoic deposits in the Pelotas Basin, South Atlantic. *Basin Research* 33, 2252–2280. <https://doi.org/10.1111/bre.12556>

This article has been peer-reviewed and is now freely available (open access) at *Tectonophysics*: <https://doi.org/10.1016/j.tecto.2026.231100>.

Rossetti, L., Lima, E.F., Waichel, B.L., Hole, M.J., Simões, M.S., Scherer, C.M.S., 2018.

Lithostratigraphy and volcanology of the Serra Geral Group, Paraná-Etendeka Igneous Province in Southern Brazil: Towards a formal stratigraphical framework. *Journal of Volcanology and Geothermal Research*. <https://doi.org/10.1016/j.jvolgeores.2017.05.008>

Sacek, V., Braun, J., van der Beek, P., 2012. The influence of rifting on escarpment migration on high elevation passive continental margins. *J. Geophys. Res.* 117. <https://doi.org/10.1029/2011jb008547>

Sacek, V., de Moraes Neto, J.M., Vasconcelos, P.M., de Oliveira Carmo, I., 2019. Numerical Modeling of Weathering, Erosion, Sedimentation, and Uplift in a Triple Junction Divergent Margin. *Geochem Geophys Geosyst* 20, 2334–2354. <https://doi.org/10.1029/2018gc008124>

Salazar-Mora, C.A., Sacek, V., 2023. Effects of Tectonic Quiescence Between Orogeny and Rifting. *Tectonics* 42. <https://doi.org/10.1029/2022tc007492>

Salgado, A.A.R., Marent, B.R., Cherem, L.F.S., Bourlès, D., Santos, L.J.C., Braucher, R., Barreto, H.N., 2013. Denudation and retreat of the Serra do Mar escarpment in southern Brazil derived from in situ-produced ^{10}Be concentration in river sediment. *Earth Surf Processes Landf.* <https://doi.org/10.1002/esp.3448>

Salgado, A.A.R., Rezende, E. de A., Bourlès, D., Braucher, R., da Silva, J.R., Garcia, R.A., 2016. Relief evolution of the Continental Rift of Southeast Brazil revealed by in situ-produced ^{10}Be concentrations in river-borne sediments. *Journal of South American Earth Sciences*. <https://doi.org/10.1016/j.jsames.2016.02.002>

Scherer, C.M.S., 2000. Eolian dunes of the Botucatu Formation (Cretaceous) in southernmost Brazil: morphology and origin. *Sedimentary Geology*. [https://doi.org/10.1016/s0037-0738\(00\)00135-4](https://doi.org/10.1016/s0037-0738(00)00135-4)

This article has been peer-reviewed and is now freely available (open access) at *Tectonophysics*:
<https://doi.org/10.1016/j.tecto.2026.231100>.

Scherer, C.M.S., Reis, A.D., Horn, B.L.D., Bertolini, G., Lavina, E.L.C., Kifumbi, C., Goso Aguilar, C., 2023. The stratigraphic puzzle of the permo-mesozoic southwestern Gondwana: The Paraná Basin record in geotectonic and palaeoclimatic context. *Earth-Science Reviews*.

<https://doi.org/10.1016/j.earscirev.2023.104397>

Silva, R.M., Sacek, V., 2019. Shallow necking depth and differential denudation linked to post-rift continental reactivation: The origin of the Cenozoic basins in southeastern Brazil. *Terra Nova* 31, 527–533.

Stica, J.M., Zalán, P.V., Ferrari, A.L., 2014. The evolution of rifting on the volcanic margin of the Pelotas Basin and the contextualization of the Paraná–Etendeka LIP in the separation of Gondwana in the South Atlantic. *Marine and Petroleum Geology*.

<https://doi.org/10.1016/j.marpetgeo.2013.10.015>

Tassara, A., Swain, C., Hackney, R., Kirby, J., 2007. Elastic thickness structure of South America estimated using wavelets and satellite-derived gravity data. *Earth and Planetary Science Letters*.

<https://doi.org/10.1016/j.epsl.2006.10.008>

Thompson, R.N., Gibson, S.A., Mitchell, J.G., Dickin, A.P., Leonardos, O.H., Brod, J.A., Greenwood, J.C., 1998. Migrating Cretaceous-Eocene Magmatism in the Serra do Mar Alkaline Province, SE Brazil: Melts from the Deflected Trindade Mantle Plume? *Journal of Petrology*.

<https://doi.org/10.1093/petro/39.8.1493>

Thybo, H., Artemieva, I.M., 2013. Moho and magmatic underplating in continental lithosphere.

Tectonophysics. <https://doi.org/10.1016/j.tecto.2013.05.032>

This article has been peer-reviewed and is now freely available (open access) at *Tectonophysics*: <https://doi.org/10.1016/j.tecto.2026.231100>.

van der Beek, P., Summerfield, M.A., Braun, J., Brown, R.W., Fleming, A., 2002. Modeling postbreakup landscape development and denudational history across the southeast African (Drakensberg Escarpment) margin. *J. Geophys. Res.* <https://doi.org/10.1029/2001jb000744>

Van Ranst, G., Pedrosa-Soares, A.C., Novo, T., Vermeesch, P., De Grave, J., 2020. New insights from low-temperature thermochronology into the tectonic and geomorphologic evolution of the southeastern Brazilian highlands and passive margin. *Geoscience Frontiers*.

<https://doi.org/10.1016/j.gsf.2019.05.011>

Veizer, J., Ala, D., Azmy, K., Bruckschen, P., Buhl, D., Bruhn, F., Carden, G.A.F., Diener, A., Ebner, S., Godderis, Y., Jasper, T., Korte, C., Pawellek, F., Podlaha, O.G., Strauss, H., 1999. $^{87}\text{Sr}/^{86}\text{Sr}$, $\delta^{13}\text{C}$ and $\delta^{18}\text{O}$ evolution of Phanerozoic seawater. *Chemical Geology*. [https://doi.org/10.1016/s0009-2541\(99\)00081-9](https://doi.org/10.1016/s0009-2541(99)00081-9)

Vieira, F., Hamza, V., 2019. Assessment of Geothermal Resources of South America - A New Look. *ijthfa*. <https://doi.org/10.31214/ijthfa.v2i1.32>

Wang, Y., Willett, S.D., 2021. Escarpment retreat rates derived from detrital cosmogenic nuclide concentrations. *Earth Surf. Dynam.* <https://doi.org/10.5194/esurf-9-1301-2021>

Wang, Y., Willett, S.D., Wu, D., Haghypour, N., Christl, M., 2021. Retreat of the Great Escarpment of Madagascar From Geomorphic Analysis and Cosmogenic ^{10}Be Concentrations. *Geochem Geophys Geosyst.* <https://doi.org/10.1029/2021gc009979>

Wildner, W., Camozzato, E., Toniolo, J.A., Binotto, R.B., Iglesias, C.M.F., Laux, J. H., 2014. Mapa geológico do estado de Santa Catarina (Technical Report, Geological Survey of Brazil, 2014); <https://rigeo.cprm.gov.br/jspui/handle/doc/17996>.

This article has been peer-reviewed and is now freely available (open access) at *Tectonophysics*:
<https://doi.org/10.1016/j.tecto.2026.231100>.

Wildner, W., Ramgrab, G.E., Lopes, R.C., Iglesias, C.M.F., 2008. Geologia e recursos minerais do estado do Rio Grande do Sul (Technical Report, Geological Survey of Brazil);

<https://rigeo.sgb.gov.br/handle/doc/10301>.

Wygrala, B. P., 1989, Integrated study of an oil field in the Southern Po-basin, Northern Italy (Ph. D. Thesis): University of Köln. (Ber. Forschungszentrum Jülich 2313, 217 pp.)